Mineralogical Magazine, October 2017, Vol. 81(5), pp. 1051–1062

Crystal chemistry of zinc incorporation in strunzite-group minerals containing zeolitic water

I. E. Grey[1,*], E. Keck[2], C. M. MacRae[1], A. M. Glenn[1], A. R. Kampf[3], B. P. Nash[4] and S. J. Mills[5]

[1] CSIRO Mineral Resources, Private Bag 10, Clayton, 3169, Victoria, Australia
[2] Algunderweg 3, D-92694 Etzenricht, Germany
[3] Mineral Sciences Department, Natural History Museum of Los Angeles County, 900 Exposition Boulevard, Los Angeles, California 90007, USA
[4] Department of Geology and Geophysics, University of Utah, Salt Lake City, Utah 84112, USA
[5] Geosciences, Museum Victoria, GPO Box 666, Melbourne 3001, Victoria, Australia

[*Received 4 August 2016; Accepted 24 September 2016; Associate Editor: G. Diego Gatta*]

ABSTRACT

A comparative study is presented of the chemistry and crystallography of zinc-bearing strunzites from Hagendorf Süd, Bavaria, Germany and the Sitio do Castelo mine, Folgosinho, Portugal. Electron microprobe analyses of samples from the two localities show quite different cation substitutions. The Hagendorf Süd mineral is a Zn-bearing ferristrunzite, with compositional zoning due to Zn^{2+} replacing predominantly Fe^{3+} as well as minor Mn^{2+}, whereas the Portugese mineral is a Zn-bearing strunzite, in which Zn^{2+} replaces Mn^{2+}, with minor replacement of Fe^{3+} by Mn^{3+}. Zincostrunzite, with dominant Zn in the interlayer octahedrally coordinated site, is a new strunzite-group mineral that has been characterized at both locations. Analysis of single-crystal synchrotron data for zinc-bearing ferristrunzite and zincostrunzite crystals from Hagendorf Süd show that the structures of both minerals contain zeolitic water in the interlayer region. The formula for strunzite-group minerals containing the zeolitic water is $M Fe_2^{3+}(PO_4)_2(OH)_2 \cdot 6.5H_2O$, M = Fe, Mn, Zn. This formulation agrees with that found for zincostrunzite from the Sitio do Castelo mine, but differs from that reported previously for strunzite, $M Fe_2^{3+}(PO_4)_2(OH)_2 \cdot 6H_2O$, which has no interlayer water. Interestingly, the zincostrunzites from the two localities differ in the location of the interlayer water molecule, with a corresponding difference in the H bonding.

Keywords: crystal chemistry of strunzites, zeolitic water in strunzites, crystallography of strunzites, zincostrunzite, Zn-bearing ferristrunzite.

Introduction

The strunzite-group minerals have been reported previously to have the general formula $M Fe_2^{3+}(PO_4)_2(OH)_2 \cdot 6H_2O$, where $M = Mn^{2+}$ in strunzite (Frondel, 1958), Fe^{2+} in ferrostrunzite (Peacor *et al.*, 1983) and Fe^{3+} in ferristrunzite (with $Fe^{3+} + OH^-$ replacing $Fe^{2+} + H_2O$, Peacor *et al.*, 1987). The minerals are of crystallo-chemical interest in having heteropolyhedral layer structures with the same layer composition as laueite-group minerals (Mills and Grey, 2015) but with different corner-linkages between the polyhedra (Krivovichev, 2004). Recently a new member of the strunzite group, zincostrunzite, with $M = Zn^{2+}$ has been reported from the Sitio do Castelo mine, Folgosinho, Portugal (Kampf *et al.*, 2016, 2017). A crystal-structure refinement for zincostrunzite revealed the presence of an interlayer water molecule, displaced slightly from the special position (½,0,0), thus changing the previously accepted formula for strunzite-group minerals to $M Fe_2^{3+}(PO_4)_2(OH)_2 \cdot 6.5H_2O$ for the case of M = Zn. The original structure analysis for strunzite (Fanfani *et al.*, 1978) found no interlayer water, and a recent structure refinement for Al-bearing

*E-mail: ian.grey@csiro.au
https://doi.org/10.1180/minmag.2016.080.151

strunzite (Grey *et al.*, 2012) also did not find interlayer water, despite the data being of high-enough quality to locate all H atoms.

In addition to the Portugese location, zincostrunzite has also been found in an oxidized phosphate zone of the Hagendorf Süd pegmatite, Bavaria (Kampf *et al.*, 2016, 2017). The Hagendorf Süd zincostrunzite occurs in zoned crystals together with zinc-bearing ferristrunzite. The zincostrunzites from the two deposits have different locations of the interlayer water molecules and different elemental substitution patterns involving zinc. We report here a comparison of the results of electron microprobe (EMP) analyses and crystal-structure refinements for the zinc-bearing strunzite-group minerals from the two localities.

Experimental

Electron microprobe analyses

Zoned crystals of Zn-bearing ferristrunzite/zincostrunzite from Hagendorf Süd were mounted in an epoxy block, polished and carbon coated for EMP analyses. The analyses were conducted using wavelength-dispersive spectrometry (WDS) on a JEOL JXA 8500F Hyperprobe operated at an accelerating voltage of 12 kV and a beam current of 4 nA. The beam was generally defocused to 2 μm for the analyses, although some of the needle-shaped crystals were so thin (≤1 μm) that a focused beam had to be used. Standards used were $AlPO_4$ for P; hematite for Fe; rhodonite for Mn and phosphophyllite for Zn. No other elements were detected by energy dispersive spectrometry (EDS). Oxygen was calculated by stoichiometry. All EMP data were corrected using a φ(ρz) matrix correction procedure implemented in the JEOL system.

Analyses of zinc-bearing strunzite and zincostrunzite crystals from the Sitio do Castelo mine, Portugal, were conducted with a Cameca SX-50 electron microprobe in WDS mode, operated at 15 kV and 10 nA with a 10 μm beam diameter, and using *Probe for EPMA* software (Probe Software Inc.). Standards were synthetic ZnO, rhodonite for Mn, hematite for Fe and fluorapatite for P. The raw analyses were corrected for matrix effects with a φ(ρz) algorithm (Pouchou and Pichoir, 1991). The EMP analyses are summarized in Table 1.

After synchrotron X-ray diffraction (XRD) data collections were made on crystals of zinc-bearing ferristrunzite and zincostrunzite from Hagendorf

TABLE 1. Summary of composition from electron microprobe analyses (wt.%).

	Ferristrunzite (18 analyses)			Zincostrunzite (7 analyses)		
Oxide	Mean	Range	SD	Mean	Range	SD
Hagendorf Süd pegmatite, Bavaria locality						
Fe_2O_3	38.5	34.1–43.0	2.3	31.3	22.7–38.6	6.2
ZnO	2.55	0.66–4.80	1.2	12.6	7.43–19.3	4.8
MnO	4.85	3.05–7.40	1.0	2.85	0.00–7.36	3.2
P_2O_5	28.0	24.2–30.3	1.8	28.2	26.8–29.3	0.83
H_2O*	25.6			25.6		
Total	99.5			100.5		
	Strunzite (10 analyses)			Zincostrunzite (12 analyses)		
Oxide	Mean	Range	SD	Mean	Range	SD
Sitio do Castelo mine, Portugal locality						
Fe_2O_3	30.5	28.9–32.1	0.7	32.0	31.2–32.8	0.4
ZnO	5.54	3.72–6.64	1.2	11.8	9.2–13.5	1.3
MnO	10.9	7.2–14.0	2.1	3.39	1.02–5.09	1.3
P_2O_5	29.3	28.6–30.1	0.3	28.8	28.1–29.4	0.3
H_2O*	25.3			26.9		
Total	101.5			102.9		

*Calculated from structure.
SD – standard deviation.

https://doi.org/10.1180/minmag.2016.080.151 Published online by Cambridge University Press

Süd, the needles were lain flat on a strip of carbon tape attached to an epoxy block, then carbon-coated and analysed by EDS using a Bruker Silicon Drift Detector on a FEI Quanta 400 field emission environmental scanning electron microscope. The EDS standards were metallic Mn and Zn, hematite for Fe and $AlPO_4$ for P.

Single-crystal X-ray diffraction

Needle-shaped crystals of zinc-bearing ferristrunzite and zincostrunzite were used for XRD data collection on the macromolecular beam line MX2 of the Australian Synchrotron. Data were collected at 100(2) K using an ADSC Quantum 315r detector and monochromatic radiation with a wavelength of 0.7100 Å. A phi scan was employed with frame-widths of 1° and a counting time per frame of 1 s. The intensity data sets were processed to produce data files which were analysed in *WinGX* (Farrugia, 1999). The refinements were made using *JANA2006* (Petříček *et al.*, 2014).

Zinc-bearing ferristrunzite

The published atomic coordinates for the non-H atoms in Al-bearing strunzite (Grey *et al.*, 2012) were used to start the refinement in the triclinic space group $P\bar{1}$. The scattering curve for Fe was used for the three independent metal atom sites. Refinement with anisotropic displacement parameters converged at $R_{obs} = 0.052$ for 3035 observed reflections. A difference-Fourier map revealed the presence of a large peak (6.4 *e* Å^{-3}), displaced by 0.43 Å from the special position (½, 0, ½). As this site is in the middle of a large cavity and not bonded to any metal atoms, it was considered to be a water molecule. Allocation of oxygen to the site, Ow7, and refinement of the site occupancy gave a value of 0.5, corresponding to full occupancy of the special position. Inclusion of Ow7 resulted in a lowering of R_{obs} to 0.037. A difference-Fourier map revealed the presence of 14 H atoms. These were included and refined with soft restraints on O–H (0.90(2) Å) and H–O–H (109.5(1)°). A single isotropic displacement parameter was refined for the H atoms. The refinement converged at $R_{obs} =$ 0.027. In the final refinement the site occupancy at *M* was set at the values obtained from the subsequent EDS analysis of the data crystal, 0.52Fe + 0.38Mn + 0.10Zn and the Fe site occupancy was allowed to refine. It did not change significantly from the starting value. Further details of the data collection and structure refinement are given in Table 2. Refined coordinates and anisotropic displacement parameters are reported in Table 3.

TABLE 2. Data collection and refinement details for Zn-bearing ferristrunzite and zincostrunzite from Hagendorf Süd.

	Zn-bearing ferristrunzite	Zincostrunzite
Formula	$MFe_2^{3+}(PO_4)_2(OH)_{2\pm x}(H_2O)_{6\pm x}\cdot 0.5H_2O$	
Occupancy of *M*	$0.52Fe^{3+} + 0.38Mn^{2+} + 0.10Zn$	$0.10Fe^{3+} + 0.10Mn^{2+} + 0.68Zn$
Temperature	100 K	100 K
Wavelength	0.7100	0.7100
Crystal system/space group	Triclinic $P\bar{1}$	Triclinic $P\bar{1}$
Unit-cell dimensions	$a = 10.123(2)$ Å $\alpha = 91.21(3)°$	$a = 10.205(2)$ Å $\alpha = 90.42(3)°$
	$b = 9.769(2)$ Å $\beta = 97.61(3)°$	$b = 9.759(2)$ Å $\beta = 98.10(3)°$
	$c = 7.312(1)$ Å $\gamma = 116.64(3)°$	$c = 7.312(1)$ Å $\gamma = 117.99(3)°$
Cell volume, *Z*	$V = 638.0(3)$ Å^3, $Z = 2$	$V = 634.4(2)$ Å^3, $Z = 2$
Density (calc.)	2.65 g cm^{-3}	2.65 g cm^{-3}
Absorption coefficient	3.61 mm^{-1}	4.03 mm^{-1}
Crystal size (mm)	0.003 × 0.003 × 0.2	0.006 × 0.009 × 0.8
Data collection resolution	0.71	0.71
Reflections collected	12,739	10,704
Independent reflections, R_{int}	3248, 0.020	3009, 0.051
Observed reflections, $I > 3\sigma(I)$	3035	2508
Data/restraints/parameters	3248/23/249	3009/20/245
R indices, observed reflections	$R_{obs} = 0.027$, $wR_{obs} = 0.039$	$R_{obs} = 0.049$, $wR_{obs} = 0.061$
R indices, all data	$R_{obs} = 0.029$, $wR_{obs} = 0.039$	$R_{obs} = 0.059$, $wR_{obs} = 0.062$
Largest difference peak and hole	+0.56 and –0.54 *e* Å^{-3}	+0.79 and –0.81 *e* Å^{-3}

https://doi.org/10.1180/minmag.2016.080.151 Published online by Cambridge University Press

TABLE 3. Atomic coordinates and displacement parameters (Å^2) for Zn-bearing ferristrunzite from Hagendorf Süd.

	x	*y*	*z*	U_{eq}	U^{11}	U^{22}	U^{33}	U^{23}	U^{13}	U^{12}
*M**	0.50509(3)	0.33242(3)	0.24313(4)	0.01486(11)	0.01525(15)	0.01406(14)	0.01864(18)	0.00820(11)	0.00751(10)	0.00530(10)
Fe1	0.96832(3)	0.24103(3)	0.13371(3)	0.00862(10)	0.01134(14)	0.00713(13)	0.00812(16)	0.00507(10)	0.00062(9)	0.00086(8)
Fe2	0.02412(3)	0.76748(3)	0.36659(3)	0.00899(10)	0.01197(14)	0.00679(13)	0.00830(16)	0.00469(10)	0.00037(9)	0.00035(9)
P1	0.81438(5)	0.47027(5)	0.06374(6)	0.00885(15)	0.01056(19)	0.00698(18)	0.0097(2)	0.00485(15)	0.00063(15)	0.00093(14)
P2	0.19289(5)	0.15029(5)	0.42841(6)	0.00884(15)	0.00955(19)	0.00634(18)	0.0105(2)	0.00380(14)	0.00042(14)	0.00103(13)
O1	0.65109(16)	0.43628(17)	0.0700(2)	0.0169(5)	0.0150(6)	0.0237(6)	0.0156(8)	0.0116(5)	0.0033(5)	0.0057(5)
O2	0.81848(15)	0.31579(14)	0.02932(19)	0.0127(4)	0.0171(6)	0.0089(5)	0.0133(7)	0.0083(5)	–0.0027(5)	–0.0010(4)
O3	0.91429(15)	0.55238(13)	0.24895(19)	0.0119(4)	0.0166(6)	0.0080(5)	0.0108(7)	0.0062(4)	–0.0002(5)	–0.0006(4)
O4	0.86212(15)	0.56634(14)	0.90018(19)	0.0137(4)	0.0173(6)	0.0091(5)	0.0116(7)	0.0037(4)	–0.0001(5)	0.0021(4)
O5	0.09985(14)	0.14671(14)	0.24080(19)	0.0111(4)	0.0145(6)	0.0105(5)	0.0101(6)	0.0076(4)	0.0005(4)	0.0006(4)
O6	0.14850(15)	0.01599(14)	0.47754(19)	0.0118(4)	0.0156(6)	0.0081(5)	0.0108(7)	0.0052(4)	–0.0002(4)	0.0002(4)
O7	0.35998(15)	0.22847(16)	0.4143(2)	0.0161(5)	0.0110(6)	0.0149(6)	0.0216(8)	0.0047(5)	0.0032(5)	0.0050(5)
O8	0.16674(14)	0.23802(14)	0.58570(19)	0.0123(4)	0.0131(6)	0.0108(5)	0.0131(7)	0.0064(4)	–0.0001(4)	–0.0018(4)
Oh1	0.95699(15)	0.30688(14)	0.38653(18)	0.0111(4)	0.0180(6)	0.0090(5)	0.0092(7)	0.0089(5)	0.0017(4)	0.0012(4)
Oh2	0.03085(15)	0.84354(14)	0.11546(18)	0.0120(4)	0.0186(6)	0.0081(5)	0.0102(7)	0.0071(4)	0.0015(5)	0.0014(4)
Ow1	0.32510(18)	0.25158(17)	0.0098(2)	0.0210(5)	0.0220(7)	0.0182(6)	0.0203(8)	0.0070(5)	0.0031(6)	0.0025(5)
Ow2	0.67263(18)	0.43128(17)	0.4788(2)	0.0201(5)	0.0243(7)	0.0229(7)	0.0141(8)	0.0113(6)	0.0041(5)	0.0039(5)
Ow3	0.48281(18)	0.53864(18)	0.2591(2)	0.0205(6)	0.0259(7)	0.0237(7)	0.0162(8)	0.0156(6)	0.0006(6)	0.0037(5)
Ow4	0.5369(2)	0.1391(2)	0.1897(3)	0.0291(7)	0.0280(8)	0.0305(8)	0.0379(11)	0.0197(7)	0.0101(7)	0.0093(7)
Ow5	0.22715(16)	0.75721(16)	0.3374(2)	0.0150(5)	0.0176(6)	0.0195(6)	0.0112(7)	0.0116(5)	0.0013(5)	0.0009(5)
Ow6	–0.22338(15)	0.03836(14)	0.16633(20)	0.0133(4)	0.0155(6)	0.0103(5)	0.0119(7)	0.0044(4)	0.0001(5)	0.0011(4)
Ow7*	0.4803(4)	0.0249(4)	0.5247(6)	0.0311(14)	0.0354(19)	0.0277(17)	0.040(2)	0.0206(14)	0.0145(15)	0.0133(15)
H01	0.949(5)	0.393(3)	0.365(6)	0.061(4)						
H02	0.048(5)	0.940(3)	0.138(6)	0.061(4)						
H1a	0.338(4)	0.307(5)	–0.087(4)	0.061(4)						
H1b	0.239(3)	0.233(5)	0.045(5)	0.061(4)						
H2a	0.641(4)	0.442(4)	0.581(4)	0.061(4)						
H2b	0.749(4)	0.516(3)	0.465(5)	0.061(4)						
H3a	0.441(4)	0.558(4)	0.154(4)	0.061(4)						
H3b	0.553(4)	0.626(3)	0.318(5)	0.061(4)						
H4a	0.619(3)	0.154(5)	0.144(5)	0.061(4)						
H4b	0.524(4)	0.077(4)	0.279(5)	0.061(4)						
H5a	0.231(5)	0.735(4)	0.219(3)	0.061(4)						
H5b	0.238(5)	0.688(4)	0.408(4)	0.061(4)						
H6a	–0.221(5)	0.021(4)	0.289(3)	0.061(4)						
H6b	–0.257(5)	–0.052(3)	0.097(4)	0.061(4)						
H7a	0.580(3)	0.080(7)	0.570(12)	0.061(4)						
H7b	0.441(8)	0.092(7)	0.492(12)	0.061(4)						

*Occupancy of $M = 0.52Fe + 0.38Mn + 0.10Zn$; occupancy of Ow7, H7a and H7b = 0.5. All other sites have full occupancy by the elements shown in the first column.

Zincostrunzite refinement

The non-H atom coordinates from the refinement of zinc-bearing ferristrunzite were used to initiate the refinement of the zincostrunzite data using space group $P\bar{1}$. The interlayer Ow7 was not included. An isotropic displacement parameter refinement gave $R_{obs} = 0.13$ and a difference-Fourier map gave the strongest peak at (0.52, –0.03, 0.47) located at 0.43 Å from the special position (½, 0, ½), corresponding to Ow7. With inclusion of Ow7, R_{obs} remained high. Application of *TwinRotMat* in *WinGX* indicated twinning by 180° rotation about the reciprocal axis [$\bar{1}$ 2 0]*. Twinning was then included in the refinement, with resulting refined twin volumes of 0.667(4) and 0.333. The *M* site was populated with 0.10Fe + 0.10Mn + 0.65Zn, as found from the subsequent EDS analyses of the data crystal. The minor Fe and Mn contents were fixed and the major Zn occupation was allowed to refine, resulting in 0.676(3) Zn in the *M* site. Anisotropic displacement parameter refinement gave $R_{obs} = 0.051$ for 2509 reflections with $I > 3\sigma(I)$. The positions of all H atoms except those associated with the disordered interlayer water molecule Ow7 were located in difference-Fourier maps. They were included in the final refinement with distance and angle restraints as for the zinc-bearing ferristrunzite, resulting in convergence at $R_{obs} = 0.049$. Further details of the data collection and refinement are given in Table 2. The refined atomic coordinates and anisotropic displacement parameters are reported in Table 4.

Results and discussion

Chemical composition of Zn-bearing ferristrunzites from Hagendorf Süd

A feature of Zn-bearing ferristrunzite needles at Hagendorf Süd is a longitudinal zoning of Zn, having a negative correlation with (Fe + Mn). This is illustrated in Fig. 1 for a typical crystal, 6 μm in diameter. The crystal was analysed at five positions along its length, ~20 μm apart. The analysis spots are evident from the beam damage. The zinc concentration displays an approximately exponential dependence on distance from the tip of the crystal, suggestive of diffusion-controlled incorporation of zinc into the crystal. The location of the Zn-enrichment was determined by *in situ* EDS analysis of crystals in a hand specimen. The analyses were conducted at low pressure to avoid charging effects. A back-scattered electron image of a typical sheaf of needle-like crystals is shown in Fig. 2. The EDS analyses confirmed that the Zn was enriched at the free ends of the needles that pointed into a cavity, and that the Zn content decreased towards the ends that were tethered to the substrate. These observations suggest that Zn diffused into the needles (or the growing needles incorporated more Zn) during immersion of the minerals in Zn-containing solutions rather than diffusion from the substrate minerals.

From the analyses of the zoned crystal shown in Fig. 1, the atom contents at each point, normalized to 3 metal atoms per formula unit (apfu), were calculated and are given in Fig. 1. Assigning 2 Fe atoms to the trivalent iron sites, Fe1 and Fe2, gives *M*-site compositions that range from $Zn_{0.9}Fe_{0.1}$ at the tip of the needle to $Zn_{0.1}Mn_{0.35}Fe_{0.55}$ at ~70 μm from the tip. It is evident that, except at the tip, the strunzite is Fe-rich rather than Mn-rich. The Zn apfu are plotted against Mn and (Fe-2) apfu in Fig. 1, showing that Zn replaces both Fe and Mn in this Zn-bearing ferristrunzite.

All 25 EMP analyses are plotted in Fig. 3 as Zn apfu *vs*. (Fe + Mn) apfu. The results show a strong negative correlation ($R^2 = 0.94$) with a linear trend-line slope close to –1. The analyses are separated in Table 1 into those with Zn dominant in the *M* site (zincostrunzite) and those that correspond to Zn-bearing ferristrunzite. The empirical formulae for the two mineral types, based on 2 P apfu and with the ratio of OH^- to H_2O in the heteropolyhedral framework adjusted for charge balance, are:

Zincostrunzite: $[Zn_{0.77}Mn^{2+}_{0.20}Fe^{3+}_{1.98}(PO_4)_2(OH)_{1.88}(H_2O)_{6.12}]0.5H_2O$

Ferristrunzite: $[Zn_{0.16}Mn^{2+}_{0.35}Fe^{3+}_{2.44}(PO_4)_2(OH)_{2.34}(H_2O)_{5.66}]0.5H_2O$

The 8 coordinated ($H_2O + OH^-$) species and the 0.5 molecules of interlayer H_2O are from the structure analysis. The formula in brackets corresponds to the heteropolyhedral framework.

The reporting of all iron as Fe^{3+} in the empirical formulae is based on the results of the structure refinements (bond-valence calculations). It is possible, however, that at the time of the zinc incorporation the iron in the *M* site was divalent (ferrostrunzite) and that oxidation of the iron occurred later.

The increase in Zn of 0.61 apfu from the mean ferristrunzite to zincostrunzite compositions is offset predominantly by a decrease in Fe of 0.46 apfu, together with a smaller decrease of 0.15 apfu of Mn. The mean compositions for both

https://doi.org/10.1180/minmag.2016.080.151 Published online by Cambridge University Press

TABLE 4. Atomic coordinates and displacement parameters (Å^2) for zincostrunzite from Hagendorf Süd.

	x	*y*	*z*	U_{eq}	U^{11}	U^{22}	U^{33}	U^{23}	U^{13}	U^{12}
*M**	0.50604(6)	0.33360(7)	0.24343(8)	0.0194(3)	0.0205(3)	0.0211(3)	0.0179(4)	0.0114(3)	0.0010(2)	0.0017(2)
Fe1	0.96727(6)	0.24118(6)	0.13477(8)	0.0164(2)	0.0209(3)	0.0169(3)	0.0126(3)	0.0110(2)	–0.0014(2)	0.0012(2)
Fe2	0.02550(6)	0.76906(6)	0.36474(8)	0.0169(2)	0.0213(3)	0.0163(3)	0.0138(3)	0.0104(2)	–0.0005(2)	0.0013(2)
P1	0.81381(11)	0.46958(12)	0.06112(14)	0.0165(4)	0.0199(4)	0.0166(5)	0.0138(5)	0.0104(4)	–0.0008(3)	0.0012(4)
P2	0.19396(11)	0.15284(12)	0.43271(14)	0.0172(4)	0.0197(4)	0.0172(5)	0.0150(6)	0.0102(4)	–0.0013(3)	0.0018(4)
O1	0.6527(4)	0.4378(4)	0.0653(5)	0.0267(13)	0.0248(14)	0.0409(19)	0.0197(17)	0.0201(14)	0.0029(12)	0.0060(13)
O2	0.8173(3)	0.3151(3)	0.0287(4)	0.0205(11)	0.0258(14)	0.0195(14)	0.0162(15)	0.0129(12)	–0.0044(11)	–0.0005(10)
O3	0.9146(3)	0.5526(3)	0.2471(4)	0.0194(11)	0.0263(14)	0.0164(13)	0.0158(15)	0.0115(12)	–0.0011(11)	0.0012(10)
O4	0.8641(3)	0.5648(3)	0.8970(4)	0.0206(11)	0.0250(14)	0.0188(14)	0.0108(15)	0.0069(12)	–0.0056(10)	–0.0017(10)
O5	0.1016(3)	0.1491(3)	0.2433(4)	0.0187(11)	0.0218(13)	0.0176(13)	0.0161(15)	0.0106(11)	–0.0030(10)	0.0010(10)
O6	0.1502(3)	–0.0142(3)	0.4781(4)	0.0196(11)	0.0244(13)	0.0177(13)	0.0154(16)	0.0101(12)	–0.0010(11)	0.0017(11)
O7	0.3620(3)	0.2356(4)	0.4265(4)	0.0230(12)	0.0208(13)	0.0226(15)	0.0234(17)	0.0089(12)	0.0015(11)	0.0068(12)
O8	0.1648(3)	0.2365(3)	0.5898(4)	0.0209(11)	0.0208(13)	0.0202(14)	0.0234(17)	0.0113(12)	0.0033(11)	0.0033(11)
Oh1	0.9561(3)	0.3068(3)	0.3880(4)	0.0191(11)	0.0269(14)	0.0192(14)	0.0152(15)	0.0147(12)	0.0021(11)	0.0037(11)
Oh2	0.0330(3)	0.8448(3)	0.1133(4)	0.0189(11)	0.0253(13)	0.0162(13)	0.0158(15)	0.0111(12)	0.0005(11)	0.0013(10)
Ow1	0.3200(4)	0.2534(4)	0.0150(5)	0.0256(13)	0.0294(15)	0.0228(15)	0.0273(18)	0.0150(13)	0.0027(13)	0.0037(13)
Ow2	0.6816(4)	0.4341(4)	0.4795(4)	0.0248(13)	0.0274(15)	0.0255(16)	0.0203(17)	0.0116(13)	0.0031(12)	0.0035(12)
Ow3	0.4854(4)	0.5433(4)	0.2645(5)	0.0295(14)	0.0402(19)	0.0272(16)	0.0204(18)	0.0185(16)	–0.0071(12)	–0.0001(13)
Ow4	0.5338(4)	0.1366(5)	0.1894(6)	0.0394(17)	0.039(2)	0.040(2)	0.046(3)	0.0266(18)	–0.0042(17)	–0.0070(17)
Ow5	0.2298(3)	0.7626(4)	0.3367(4)	0.0233(12)	0.0274(14)	0.0317(17)	0.0168(16)	0.0199(14)	0.0002(11)	0.0017(12)
Ow6	–0.2240(3)	0.0366(3)	0.1653(4)	0.0218(12)	0.0274(14)	0.0182(14)	0.0168(16)	0.0096(12)	–0.0006(11)	0.0015(11)
Ow7*	0.5245(9)	0.9779(11)	0.4808(13)	0.043(4)	0.039(4)	0.052(5)	0.045(5)	0.027(4)	0.007(3)	0.010(4)
H01	0.936(9)	0.385(6)	0.360(10)	0.064(6)						
H02	0.044(9)	0.941(4)	0.128(11)	0.064(6)						
H1a	0.340(7)	0.344(5)	–0.036(10)	0.064(6)						
H1b	0.230(5)	0.214(7)	0.054(10)	0.064(6)						
H2a	0.652(7)	0.462(7)	0.576(7)	0.064(6)						
H2b	0.767(5)	0.513(5)	0.458(9)	0.064(6)						
H3a	0.444(8)	0.562(7)	0.158(6)	0.064(6)						
H3b	0.545(8)	0.633(4)	0.334(8)	0.064(6)						
H4a	0.556(9)	0.074(7)	0.123(8)	0.064(6)						
H4b	0.516(9)	0.101(8)	0.300(5)	0.064(6)						
H5a	0.231(9)	0.739(8)	0.217(4)	0.064(6)						
H5b	0.231(10)	0.688(6)	0.405(7)	0.064(6)						
H6a	–0.215(9)	0.021(7)	0.287(3)	0.064(6)						
H6b	–0.255(9)	–0.053(4)	0.097(7)	0.064(6)						

*Occupancy of *M* = 0.676(3) Zn + 0.1 Mn + 0.1 Fe; Ow7 = 0.5. All other sites have full occupation.

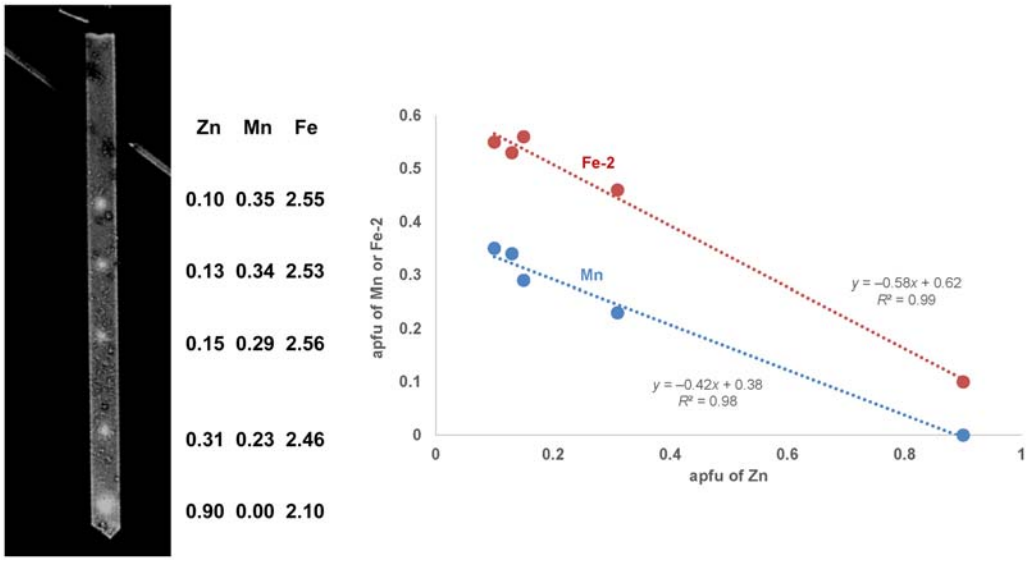

FIG. 1. Electron microprobe results (atoms per formula unit) for a zoned crystal of Zn-bearing ferristrunzite from Hagendorf Süd.

types of strunzite have a small deficiency in the number of metal atoms, with $3 - \Sigma M = 0.05$. Vacancies at the *M* site in zincostrunzite were confirmed in the structure refinement and are reported below. Small concentrations of vacancies are commonly reported for iron phosphate minerals as discussed by Kolitsch *et al.* (2010).

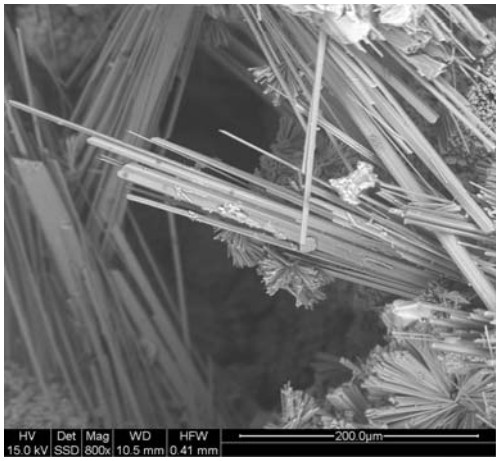

FIG. 2. Zn-bearing ferristrunzite crystals in hand specimen from Hagendorf Süd. The associated fan-like clusters are crystals of whitmoreite/earlshannonite.

Chemical composition of Zn-bearing strunzites from Portugal

Zn-bearing strunzite from the Sitio do Castelo mine, Portugal, shows a significantly different mode of Zn substitution to that from Hagendorf Süd. Results from EMP analyses for this sample are summarized in Table 1. As for the Hagendorf Süd sample, considerable compositional zoning occurs within individual crystals, and the results in Table 1 have been separated into those where Zn is the dominant component in the *M* site (zincostrunzite) and those in which Mn is dominant in the *M* site (Zn-bearing strunzite). In contrast to the Hagendorf Süd ferristrunzite crystals, with >2 Fe apfu, the Portugese mineral has Fe almost invariant at 2 Fe apfu in the Zn-bearing strunzite and has <2 Fe apfu in the zincostrunzite. A possible interpretation is that some Mn^{3+} replaces Fe^{3+} in the Zn-bearing strunzite. In support of this, a plot of Fe apfu *vs.* Mn apfu for the strunzite results shows a negative correlation with a slope of –1.2, whereas Fe *vs.* Zn shows only a very weak positive correlation. On the basis of Mn^{3+} completing the occupancy of the Fe^{3+} sites, the empirical formulae for the two mineral types have been calculated from the average EMP analyses and are given below. Consistent with the formulae calculated for the Hagendorf Sud samples, charge balance is achieved

https://doi.org/10.1180/minmag.2016.080.151 Published online by Cambridge University Press

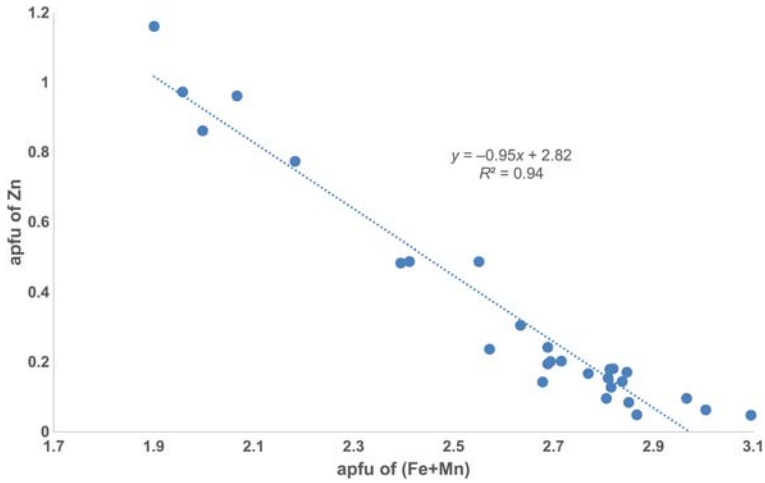

FIG. 3. Plot of atoms of Zn apfu *vs.* Fe + Mn apfu, using EMP results for Zn-bearing ferristrunzite and zincostrunzite from Hagendorf Süd.

by adjusting the ratio of OH^- to H_2O for the heteropolyhedral framework and the zeolitic water is shown outside the brackets.

Zincostrunzite: $[Zn_{0.72}Mn^{2+}_{0.22}(Fe^{3+}_{1.98}Mn^{3+}_{0.02})(PO_4)_2(OH)_{1.88}(H_2O)_{6.12}]0.5H_2O$

Strunzite: $Zn_{0.33}Mn^{2+}_{0.61}(Fe^{3+}_{1.87}Mn^{3+}_{0.13})(PO_4)_2(OH)_{1.88}(H_2O)_{6.12}]0.5H_2O$

The change of mean composition between strunzite and zincostrunzite involves Mn^{3+}/Fe^{3+} substitution at the Fe^{3+} sites and Mn^{2+}/Zn substitution at the *M* site. A plot of Mn apfu *vs.* (Fe + Zn) apfu for all EMP data is fitted very well ($R^2 = 0.97$) by a linear trendline with a slope of –1, shown in Fig. 4. When the Fe is not taken into account, a trendline fit to a plot of Mn *vs.* Zn has a slope of –1.3, indicating that other factors are in play.

Crystal structures

The structure of strunzite-group minerals has been described in detail by Fanfani *et al.* (1978) and by

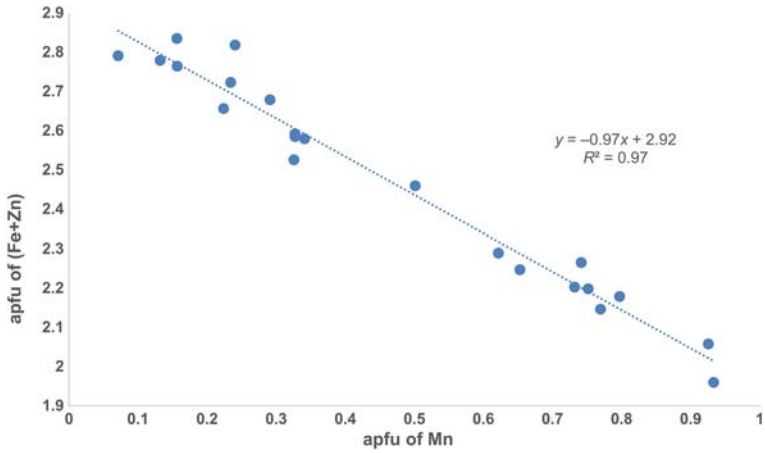

FIG. 4. Plot of Mn apfu *vs*. Fe + Zn apfu using EMP data for Zn-bearing strunzite and zincostrunzite from Sitio do Castelo, Portugal.

https://doi.org/10.1180/minmag.2016.080.151 Published online by Cambridge University Press

Grey *et al.* (2012). The heteropolyhedral framework of strunzite has the same composition as that of laueite-group minerals (Mills and Grey, 2015), and Krivovichev (2004) has described it as a topological isomer of the laueite structure. Both structures contain 7 Å chains of corner-connected Fe^{3+}-centred octahedra that are interconnected via corner-sharing with PO_4 tetrahedra to form sheets of composition $[Fe_2(OH)_2(H_2O)_2(PO_4)_2]^{2-}$. In laueite the two independent Fe^{3+}-centred octahedra have compositions $Fe(Op)_2(OH)_2(H_2O)_2$ and $Fe(Op)_4(OH)_2$ with coordination to 2 and 4 PO_4 tetrahedra respectively, whereas in strunzite both Fe^{3+}-centred octahedra have the same composition $Fe(Op)_3(OH)_2(H_2O)$ with coordination to 3 PO_4 tetrahedra. It is this different octahedral-tetrahedral linkage in the sheets that distinguishes the laueite and strunzite sheets as topological isomers (Krivovichev, 2004).

The (100) heteropolyhedral sheets in strunzite are interconnected via *M*-centred octahedra of composition $M(Op)_2(H_2O)_4$ that corner-share with PO_4 tetrahedra in the sheets. In strunzite (Fanfani *et al.*, 1978) the *M* site is considered to be occupied only by Mn^{2+} although no chemical analysis was given; the mean *M*–O distance is 2.15 Å. In Al-bearing strunzite (Grey *et al.*, 2012) The *M* site contain $0.65Mn^{2+} + 0.26Fe^{2+} + 0.08Zn + 0.01Mg$ and the mean *M*–O distance is 2.16 Å. In Zn-bearing ferristrunzite from Hagendorf Süd the mean *M*–O distance is much shorter at 2.08 Å as shown in Table 5. Based on the EDS-derived occupation of $M = 0.52Fe + 0.38Mn + 0.1Zn$, the calculated bond-valence sum is 2.59, which is consistent with the iron being in the ferric state. The Zn-bearing mineral is thus a ferristrunzite, analogous to that reported from Blaton, Belgium by Peacor *et al.* (1987).

A feature of both the Zn-bearing ferristrunzite and zincostrunzite structures that has not previously been reported is the presence of an interlayer water molecule, Ow7. It is disordered (split) over two

TABLE 5. Selected bond distances (Å) and cation-valence sums for Zn-bearing ferristrunzite (A) and zincostrunzite (B) from Hagendorf Süd.

	A	B		A	B
M–O(7)	1.989(2)	2.030(3)	Fe(1)–O(4)	1.946(2)	1.913(3)
M–O(1)	2.005(2)	2.027(4)	Fe(1)–OH1	1.978(2)	1.991(3)
M–Ow4	2.090(2)	2.113(5)	Fe(1)–OH2	1.987(2)	1.992(3)
M–Ow2	2.112(2)	2.146(3)	Fe(1)–O(5)	2.022(2)	2.043(4)
M–Ow3	2.128(2)	2.160(5)	Fe(1)–O(2)	2.032(2)	2.043(4)
M–Ow1	2.166(2)	2.168(4)	Fe(1)–Ow6	2.107(2)	2.078(3)
Average	2.082	2.107	Average	2.012	2.010
Valence sum*	2.59	2.18	Valence sum	3.06	3.07
P(1)–O(4)	1.529(2)	1.520(3)	Fe(2)–OH1	1.978(2)	1.976(3)
P(1)–O(3)	1.538(2)	1.540(3)	Fe(2)–O(8)	1.987(2)	1.992(4)
P(1)–O(1)	1.540(2)	1.529(4)	Fe(2)–O(3)	1.991(2)	1.983(3)
P(1)–O(2)	1.544(1)	1.542(4)	Fe(2)–OH2	1.994(2)	1.985(3)
Average	1.538	1.530	Fe(2)–O(6)	1.997(2)	1.983(3)
Valence sum	4.96	5.03	Fe(2)–Ow5	2.139(2)	2.153(4)
			Average	2.014	2.012
			Valence sum	3.04	3.07
P(2)–O(7)	1.532(2)	1.522(3)			
P(2)–O(8)	1.539(2)	1.544(4)			
P(2)–O(6)	1.543(2)	1.527(3)			
P(2)–O(5)	1.548(2)	1.552(3)			
Average	1.540	1.536			
Valence sum	4.92	4.98			

*Calculated using $M = 0.52Fe^{3+} + 0.38\ Mn^{2+} + 0.1Zn$ in Zn-bearing ferristrunzite and $M = 0.10Fe^{3+}\ 0.10Mn^{2+} + 0.68Zn$ in zincostrunzite. Bond-valence parameters from Brown and Altermatt (1985).

https://doi.org/10.1180/minmag.2016.080.151 Published online by Cambridge University Press

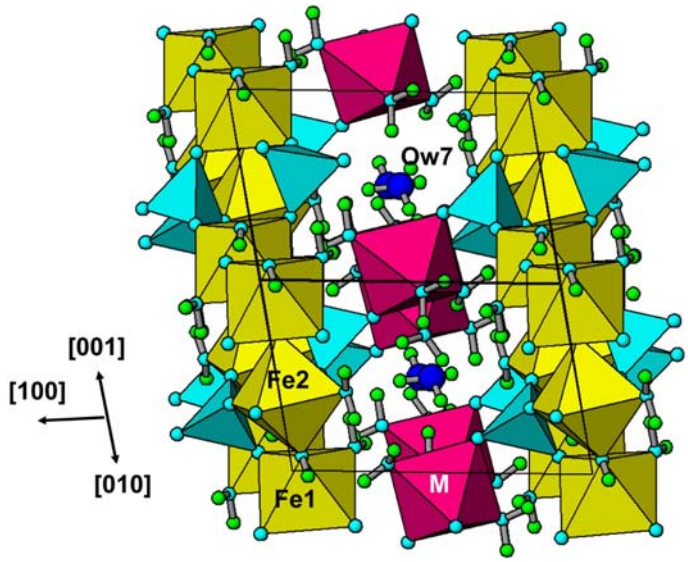

FIG. 5. [011] projection of Hagendorf Süd zincostrunzite structure. The unit cell is outlined.

sites displaced by 0.43 Å from the special position (½, 0, ½), giving an Ow7–Ow7 separation of 0.86 Å. The Ow7 molecules occupy channels directed along [011] as shown in Fig. 5. They are held by a system of H bonds involving mainly coordinated water molecules. A more detailed discussion of interlayer water in strunzite is given in the following section.

The H bonds in Zn-bearing ferristrunzite are reported in Table 6. The same H bonds were found for zincostrunzite. The H bonds generally conform to the H-bonding scheme reported for Al-bearing

TABLE 6. Hydrogen bonds for Zn-bearing ferristrunzite from Hagendorf Süd [Å and °].

D–H···*A*	*d*(*D*–H)	*d*(H···*A*)	*d*(*D*···*A*)	<(*D*H*A*)
OH1–HOH1···O(3)	0.90(4)	1.93(4)	2.805(2)	164(4)
OH2–HOH2···O(5)	0.88(3)	1.95(3)	2.821(2)	168(4)
OW1–H(1B)···O(5)	0.89(3)	2.06(4)	2.846(3)	147(4)
OW1–H(1A)···OW3	0.89(4)	2.32(3)	3.075(3)	143(4)
OW2–H(2B)···O(3)	0.86(4)	2.37(4)	2.964(3)	127(3)
OW2–H(2A)···OW3	0.87(4)	1.89(4)	2.724(3)	160(4)
OW2–H(2B)···O(8)	0.86(3)	2.22(3)	2.977(3)	146(4)
OW3–H(3B)···O(7)	0.88(2)	2.22(3)	2.988(3)	145(3)
OW3–H(3A)···O(1)	0.90(3)	1.79(3)	2.673(2)	170(4)
OW4–H(4A)···O(2)	0.89(4)	2.22(3)	3.006(3)	148(4)
OW4–H(4B)···OW7	0.89(4)	1.93(4)	2.736(5)	150(4)
OW4–H(4A)···OW6	0.89(4)	2.33(5)	3.022(3)	135(4)
OW4–H(4B)···OW7	0.89(4)	1.93(2)	2.736(5)	150(4)
OW5–H(5A)···O(2)	0.90(3)	1.82(2)	2.685(2)	162(5)
OW5–H(5B)···OW2	0.90(4)	1.91(5)	2.765(3)	159(4)
OW6–H(6A)···O(6)	0.91(2)	1.78(3)	2.656(2)	160(4)
OW6–H(6B)···OW1	0.90(3)	1.87(3)	2.760(3)	170(3)
OW7–H(7A)···OW5	0.92(3)	1.90(4)	2.790(4)	163(7)
OW7–H(7B)···O(7)	0.92(8)	1.92(8)	2.810(5)	178(8)

https://doi.org/10.1180/minmag.2016.080.151 Published online by Cambridge University Press

strunzite (Grey *et al.*, 2012). The exception is for Ow4, which is coordinated to *M* and has no H bonds with O···O shorter than 3.0 Å in Al-bearing strunzite. Due to strong H bonding with Ow7 in Zn-bearing ferristrunzite, Ow4 is considerably displaced relative to its position in Al-strunzite and forms H bonds also to O2 and Ow6. The interlayer water molecule Ow7 is a donor in H bonding to O7 and Ow5, and an acceptor in H bonds from Ow4.

Zeolitic water in strunzite

In their structure determination for strunzite, Fanfani *et al.* (1978) found no zeolitic water. In fact they comment that "*the lack of zeolitic water in the inter-slab space in strunzite causes significantly shorter separation in adjacent sheets*" (relative to laueite, pseudolaueite and stewartite). The inter-sheet separation in strunzite is 9.0 Å compared with 9.9–10.0 Å in the other three minerals. This argument has not been borne out by our results, with the interlayer separation, $d(100) = 8.93$ Å and 8.94 Å for Zn-bearing ferristrunzite and zincostrunzite respectively, both of which contain zeolitic water.

The structure analysis of Al-bearing strunzite by Grey *et al.* (2012) also did not reveal the presence of any interlayer water, despite the refinement being of high-enough quality to be able to locate all H atoms in difference-Fourier maps. Although a structure refinement was not reported for ferristrunzite by Peacor *et al.* (1987), they measured the water content by thermal analysis and obtained 26.3 wt.% H_2O. Their empirical formula is $[Fe^{3+}_{0.92}Fe^{3+}_2(PO_4)_2(OH)_{2.76}(H_2O)_{5.24}]0.64H_2O$, which is consistent with our results for Zn-bearing ferristrunzite and strongly suggestive of interlayer water in the ferristrunzite structure. The only crystal-chemical feature that appears to distinguish strunzite-group minerals with or without interlayer water is the size of the *M*-centred octahedron. Both strunzite and Al-bearing strunzite have the larger Mn^{2+} cation dominant in *M*, while the minerals that contain interlayer water have the smaller Fe^{3+} or Zn dominant in *M*.

An interesting structural distinction exists between zincostrunzite from the two localities regarding the location of the interlayer water molecule. In zincostrunzite from Hagendorf Süd, Ow7 is displaced slightly from the special position (½, 0, ½), while in zincostrunzite from the Sitio do Castelo mine, Ow7 is displaced from the special position (½, 0, 0). In the former case the Ow7 molecules occupy channels directed along [011] as shown in Fig. 5, whereas in the latter they are in channels directed along [0$\bar{1}$1]. The Ow7–Ow7 separations are the same for the two cases but the H bonding is different due to the different Ow7 locations. In the Hagendorf Süd zincostrunzite, Ow7 is a donor to Ow5 and O7, whereas in the Portugese zincostrunzite, Ow7 is a donor to Ow6 and O1. The different H bonding influences the coordination of these acceptors. In the Hagendorf

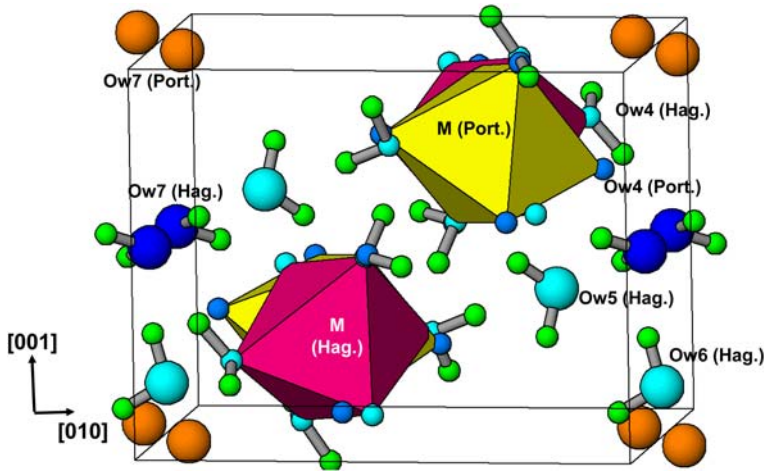

FIG. 6. [100] projection of interlayer region, with superimposed *M*-centred octahedra for zincostrunzite from Hagendorf Süd (Hag.) and Portugese (Port.) localities, to illustrate the twisting of the *M*-centred octahedra in response to different Ow7 locations.

https://doi.org/10.1180/minmag.2016.080.151 Published online by Cambridge University Press

Süd mineral, Fe2−Ow5 is longer, 2.153(4) Å, than Fe1−Ow6, 2.079(3) Å, whereas in zincostrunzite from the Sitio do Castelo mine, this is reversed and Fe2−Ow5, 2.060(8) Å is considerably shorter than Fe1−Ow6, 2.204(9) Å. In strunzite and Al-bearing strunzite, which do not contain interlayer water, the Fe1−Ow6 and Fe2−Ow5 distances are almost equal.

The different H-bonding geometry associated with the different locations of the Ow7 molecules in zincostrunzite from the two localities entails considerable twisting of the *M*-centred octahedron. This is shown in Fig. 6, a superimposed projection along [100] of the interlayer region. The *M*-centred octahedra in zincostrunzite from Hagendorf Süd and Portugese localities are shown by the dark and light colours, respectively. The twisting of the octahedra involves a large displacement of Ow4, by 1.17 Å. Ow4 is a H-bond donor to Ow7 in both structures and requires a large displacement to achieve the H bonding. The distance of Ow4 to the alternative Ow7 site near (½, 0, 0) is only 1.7 Å, so both Ow7 sites cannot be occupied in the same unit cell.

The energy difference between the two alternative Ow7 sites is likely to be very small and it is surprising that the structures do not display a disordered mixture of the two types of water molecule locations. Presumably it is because the large twisting of the *M*-centred octahedron associated with a particular location prevents it from H-bonding to a molecule in the other location, so that once a particular site is occupied it precludes occupation in the other site within the crystal.

Acknowledgements

The XRD data sets were collected at the microfocus beam line MX2 at the Australian Synchrotron. We thank the MX2 beam line scientists for help in the data collections. Thanks to Cameron Davidson for EMP sample preparation.

References

Brown, I.D. and Altermatt, D. (1985) Bond-valence parameters from a systematic analysis of the inorganic crystal structure database. *Acta Crystallographica*, **B41**, 244–247.

Fanfani, L., Tomassini, M., Zanazzi, P.F. and Zanzari, A. R. (1978) The crystal structure of strunzite, a contribution to the crystal chemistry of basic ferric-manganous hydrated phosphates. *Tschermaks Mineralogische und Petrographische Mitteilungen*, **25**, 77–87.

Farrugia, L.J. (1999) WinGX suite for small-molecule single-crystal crystallography. *Journal of Applied Crystallography*, **32**, 837–838.

Frondel, C. (1958) Strunzite, a new mineral. *Naturwissenschaften*, **45**, 37–38.

Grey, I.E, MacRae, C.M., Keck, E. and Birch, W.D. (2012) Aluminium-bearing strunzite derived from jahnsite at the Hagendorf-Süd pegmatite, Germany. *Mineralogical Magazine*, **76**, 1165–1174.

Kampf, A.R., Grey, I.E., Alves, P., Mills, S.J., Nash, B.P., MacRae, C.M. and Keck, E. (2016) Zincostrunzite, IMA 2016-023. CNMNC Newsletter No. 32, August 2016, page 918; *Mineralogical Magazine*, **80**, 915–922.

Kampf, A.R., Grey, I.E., Alves, P., Mills, S.J., Nash, B.P., MacRae, C.M. and Keck, E. (2017) Zincostrunzite, $ZnFe_2^{3+}(PO_4)_2(OH)_2{\cdot}6.5H_2O$, a new mineral from the Sitio do Castelo mine, Portugal, and the Hagendorf-Süd pegmatite, Germany. *European Journal of Mineralogy*, **29**, 315–322.

Kolitsch, U., Atencio, D., Chukanov, N.V., Zubkova, N. V., Menezes Filho, A.D., Coutinho, J.M.V., Birch, W. D., Schlüter, J., Kampf, A.R., Steele, I.M., Favreau, G., Nasdala, L., Möckel, S., Giester, G. and Pushcharovsky, D.Yu. (2010) Bendadaite, a new iron arsenate mineral of the arthurite group. *Mineralogical Magazine*, **74**, 469–486.

Krivovichev, S.V. (2004) Topological and geometrical isomerism in minerals and inorganic compounds with laueite-type heteropolyhedral sheets. *Neues Jahrbuch für Mineralogie Monatshefte*, **2004**, 209–220.

Mills, S.J. and Grey, I.E. (2015) Nomenclature for the laueite supergroup. *Mineralogical Magazine*, **79**, 243–246.

Peacor, D.R., Dunn, P.J. and Simmons, W.B. (1983) Ferrostrunzite, the ferrous iron analogue of strunzite from Mullica Hill, New Jersey. *Neues Jahrbuch für Mineralogie Monatshefte*, **1983**, 524–528.

Peacor, D.R., Dunn, P.J., Simmons, W.B. and Ramik, R.A. (1987) Ferristrunzite, a new member of the strunzite group, from Blaton, Belgium. *Neues Jahrbuch für Mineralogie Monatshefte*, **1987**, 453–457.

Petříček, V., Dušek, M. and Palatinus, L. (2014) Crystallographic Computing System JANA2006: General features. *Zeitschrift für Kristallographie*, **229**, 345–352.

Pouchou, J.-L. and Pichoir, F. (1991) Quantitative analysis of homogeneous or stratified microvolumes applying the model "PAP". Pp. 31–75 in: *Electron Probe Quantitation* (K.F.J. Heinrich and D.E. Newbury, editors). Plenum Press, New York.

https://doi.org/10.1180/minmag.2016.080.151 Published online by Cambridge University Press